Regular Article

PHYSICAL CHEMISTRY RESEARCH
Published by the
Iranian Chemical Society
www.physchemres.org
info@physchemres.org

Phys. Chem. Res., Vol. 14, No. 1, 43-59, March 2026
DOI: 10.22036/pcr.2025.545590.2740

A Comprehensive Theoretical Analysis of Carmustine Interaction with Graphene and Boron Carbon Nitride Nanoflakes: Implications of Solvent Dynamics from DFT and AIM Studies

M. Rezaei Sameti* and K. Nikkho

Department of Applied Chemistry, Faculty of Science, Malayer University, Malayer, 65174, Iran

(Received 6 September 2025, Accepted 24 November 2025)

Targeted drug delivery remains a central challenge in modern therapeutics, aiming to maximize efficacy while minimizing side effects. Nanomaterials, especially graphene and its derivatives, are promising candidates for drug delivery systems. Herein, density functional theory (DFT) calculations at the ωB97XD/6-31G(d,p) level were employed to investigate the adsorption of Carmustine (Cm), an anticancer agent, on graphene, BC3, and NC3 nanoflakes. Structural optimization and adsorption energy (E_{ads}) analyses reveal that NC3 exhibits stronger adsorption toward Cm compared with BC3 and graphene, suggesting superior carrier potential. The spontaneity of adsorption is confirmed by negative Gibbs free energy (ΔG) values in both gas and aqueous phases. Electronic structure analyses indicate the stability order Cm&BC3 < Cm&NC3 < Cm&G, highlighting BC3 and NC3 as suitable for sensitive drug-tracking sensors. Further insights from electron localization function (ELF), atoms in molecules (AIM), and reduced density gradient (RDG) analyses confirm predominantly non-covalent, electrostatic interactions. Ultraviolet-visible (UV-Vis) spectra exhibit notable shifts, supporting the feasibility of monitoring Cm within biological systems. These findings identify NC3 and BC3 nanoflakes as promising candidates for advanced drug delivery and tracking applications.

Keywords: Carmustine drug, Graphene, NC_3 and BC_3 nanoflakes, DFT, AIM

INTRODUCTION

Nanotechnology has transformed drug delivery systems by providing innovative strategies to enhance the therapeutic efficacy and safety of pharmacological agents. Among various nanomaterials, graphene and its derivatives have gained considerable attention due to their exceptional physicochemical properties, including a high surface area, superior mechanical strength, and excellent electrical conductivity [1,2]. The two-dimensional nature of graphene, coupled with these unique characteristics, has enabled its widespread application in biomedicine and materials science [3,4]. Graphene-based nanoparticles, in particular, have emerged as promising candidates for drug delivery due to their high drug-loading capacity, biocompatibility, and tunable surface chemistry [5-7]. For instance, Gong *et al*. systematically investigated the interactions of graphene and graphene oxide with various therapeutic agents, such as anastrozole, camptothecin, gefitinib, and resveratrol, providing critical insights into their adsorption mechanisms and interaction dynamics [8]. Furthermore, studies on the adsorption of biologically active molecules such as dopamine, pramipexole, and risperidone onto graphene nanostructures have elucidated the role of charge transfer processes and the distinct adsorption behaviors of agonists and antagonists based on their electronic properties [9-11]. These findings have significantly advanced the understanding of drug-nanomaterial interactions, facilitating the development of more efficient drug-delivery platforms. Beyond graphene, other nanomaterials such as nitrogen

*Corresponding author. E-mail: mrsameti@malayeru.ac.ir

carbide (NC_3), boron carbide (BC_3), and boron nitride (BN) have been extensively investigated for their potential in drug delivery and sensing applications. The adsorption energies of drug molecules on these materials play a crucial role in determining their suitability for biomedical applications. For instance, BC_3 nanoflakes have demonstrated stable adsorption of the antidiabetic drug miglitol (MT), highlighting their potential as effective drug carriers [12]. Additionally, while pristine BC_3 nanoflakes exhibit weak interactions with paracetamol (PC), platinum-decorated BC_3 nanoflakes significantly enhance the sensing response to PC through strong chemisorption processes, making them promising candidates for drug detection technologies [13,14]. Notably, NC_3 nanoflakes have also been explored for their antibacterial properties, which stem from their ability to disrupt bacterial membranes, akin to the mechanisms observed in graphene [15]. Akter Bithe *et al*. further demonstrated the efficacy of BC_3 nanoflakes in adsorbing miglitol, underscoring their potential in targeted drug delivery applications [16]. Carmustine (Cm), an alkylating agent widely used in chemotherapy, is primarily employed in the treatment of brain tumors, including glioblastoma multiforme and metastatic brain tumors, as well as Hodgkin's lymphoma and multiple myeloma [17-19]. Its mechanism of action involves forming hydrogen bonds with DNA pyrimidine bases, leading to stable molecular configurations and enhanced aqueous solubility [20]. The exothermic nature of these interactions, coupled with favorable binding energies, underscores the stability of Carmustine-nucleobase complexes. Intermolecular hydrogen bonding plays a pivotal role in stabilizing these physisorption configurations, as evidenced by negative stability energies and increased solubility in aqueous media [21,22]. In related studies, Rostamian *et al*. explored the adsorption of tetracycline drugs on graphene nanoflakes, revealing that π-π stacking and electrostatic interactions dominate the adsorption process, positioning graphene as a promising adsorbent for pharmaceutical removal from aqueous environments [23]. Similarly, Khorram *et al*. examined the interactions of Carmustine with γ-Fe_2O_3 nanoparticles and carboxyl-functionalized single-walled carbon nanotubes, demonstrating that while the interaction with γ-Fe_2O_3 is weak and primarily physisorptive, functionalized nanotubes exhibit strong hydrogen bonding, thereby stabilizing the adsorption configurations [24,25]. Soleymanabadi *et al*. investigated the potential of C_4B_{32} nanoclusters as high-capacity carriers for Carmustine, revealing that lithium doping significantly enhances the drug adsorption capacity, suggesting their utility in drug delivery systems [26]. Wolski *et al*. designed a nanocontainer capable of encapsulating hydrolytically labile molecules, such as Carmustine, to facilitate selective endocytosis by cancer cells and enable controlled drug release through external magnetic fields. However, their findings indicated that very small magnetic nanoparticles cannot generate sufficient torque to induce structural changes in the nanocontainer, limiting its functionality [27]. In a related study, Hoelm *et al.* demonstrated that the non-toxic compound 1,10-N,N-bis-(β-D-ureidocellobiosyl)-4,7,13,16-tetraoxide-1,10-diazacyclooctadecane (TN) forms stable complexes with Carmustine, effectively reducing its cytotoxic effects on normal cells [28]. Yi *et al*. developed a Carmustine-loaded poly (lactic-co-glycolic acid) (PLGA) bio-composite sphere incorporating bioactive nanoparticles for targeted glioma therapy, highlighting its potential as an innovative therapeutic strategy [29]. Khanizadeh *et al* explored the use of Carmustine-loaded nanocarriers for targeted delivery to brain tumors [30], while Majumder *et al* demonstrated that functionalized carbon nano-onions (*f*-CNO) enhance Carmustine's bioavailability and selectively target cancer cells, establishing *f*-CNO as a promising platform for intelligent chemotherapeutic delivery [31]. Rahimi *et al*. investigated the adsorption of drug molecules on a pure B_3O_3 sheet, observing a 28-32% reduction in the band gap, which suggests its potential utility as an effective drug sensor [32]. Kamel *et al*. studied the stability and electronic properties of hydroxyurea and Carmustine on both pristine and chitosan-functionalized graphitic carbon nitride (g-C_3N_4), proposing g-C_3N_4 as a viable drug delivery system for cancer treatment [33]. Additionally, Bin Iqbal *et al.* examined the adsorption behavior of nitrosourea and Carmustine on silicon carbide (SiC) nanosheets, revealing that the adsorption process is both spontaneous and energetically favorable [34]. Amiri Dolatabad *et al.* evaluated the potential of hexa-peri-hexabenzocoronene (HBC) for Carmustine sensing and delivery, reporting adsorption energies of -17.1 kcal mol^{-1} for HBC-BCNU, -17.0 kcal mol^{-1} for NHBC-BCNU, and -17.9 kcal mol^{-1} for BNHBC-BCNU using the

6-31+G(d) basis set [35]. Begum *et al* demonstrated that Carmustine interacts with the active site of glutathione reductase (GR) with negative binding energy, indicating a stable interaction [36]. Their subsequent research identified the N7 site of guanine in the DNA major groove as the preferred binding site for Carmustine [37]. Saikia *et al.* investigated the molecular interactions between Carmustine and melatonin, concluding that hydrogen bonding is the primary interaction mechanism [38]. Furthermore, Xiao *et al*. demonstrated that combining superparamagnetic γ-Fe_2O_3 nanoparticles with Carmustine significantly enhances its therapeutic efficacy against cervical carcinoma [39]. Building on our prior research into drug-nanomaterial interactions [40-47], this study aims to systematically investigate the interaction of Carmustine with graphene, BC_3, and NC_3 nanoflakes using density functional theory (DFT). Structural parameters, adsorption energies, and thermodynamic properties will be analyzed in both gaseous and aqueous phases, while topological and quantum parameters will be derived from Atoms in Molecules (AIM) analysis. The results of this study are expected to provide critical insights into the development of advanced nanomaterial-based drug delivery systems, optimizing the targeted delivery of Carmustine to improve its therapeutic outcomes.

COMPUTATIONAL DETAILS

In this study, the interaction of the Carmustine drug (Cm-drug) with graphene, BC_3, and NC_3 nanoflakes in the presence of a water solvent is systematically investigated using density functional theory (DFT). All structural optimizations are performed at the ωB97XD level of theory with the 6-31G(d,p) basis set. The ωB97XD functional incorporates 22% Hartree-Fock exchange at short ranges and 100% Hartree-Fock exchange at long ranges, ensuring an accurate description of both dispersion interactions and long-range electronic effects [48]. Structural visualization and design are conducted using GaussView 06 [49] and Chemcraft graphical software [50], while all DFT calculations are executed using the Gaussian 09 software package [51]. The optimization process adheres to stringent convergence criteria, with maximum force and displacement thresholds set at 0.00045 Hartree and 0.0018 Hartree/Bohr, respectively. The absence of imaginary frequencies in the vibrational spectra of all optimized complexes confirms their structural stability. The adsorption energy (E_{ads}) for each system is calculated using Eq. (1), providing quantitative insights into the interaction strength between the Cm-drug and the nanoflakes:

$$E_{ads} = E_{Cm\&nanoflake} - (E_{Cm} + E_{nanoflake}) + BSSE \quad (1)$$

In Eq. (1), $E_{Cm\&nanonanoflake}$, E_{Cm}, and $E_{nanoflake}$ represent the total potential electronic energy of the Cm-drug&nanoflakes (G, BC_3, and NC_3), Cm-drug, and nanoflake, respectively. The term BSSE denotes the basis set superposition error. In this study, all calculated E_{ads} energies undergo correction with BSSE, and the adjusted results are presented in Table 1.

Additionally, the ΔH and ΔG energies of the Cm&G, Cm&BC_3, and Cm&NC_3 complexes are computed using Eqs. (2) and (3), respectively. These calculated energies are also presented in Table 1 for comprehensive analysis.

$$\Delta H = H_{CP\&nanosheet} - (H_{CP} + H_{nanosheet}) \quad (2)$$

$$\Delta G = G_{CP\&nanosheet} - (G_{CP} + G_{nanosheet}) \quad (3)$$

To investigate the electronic properties of the Cm&G, Cm&BC_3, and Cm&NC_3 complexes, quantum descriptors such as the energy gap (E_{gap}), chemical potential (μ), and chemical hardness (η) were calculated based on the highest occupied molecular orbital (HOMO) and lowest unoccupied molecular orbital (LUMO) energies [52-53]. In addition, a comprehensive analysis was performed, including Electron Localization Function (ELF), Atoms in Molecules (AIM), and Reduced Density Gradient (RDG) [54-57]. Solvent effects and UV-visible spectra were also examined for all studied configurations [58-59], with detailed analysis provided for the obtained results.

RESULTS AND DISCUSSION

Structures and Thermodynamic Properties

This study systematically explores the interaction of the Carmustine (Cm) drug with graphene (G), BC_3 (B), and NC_3 (N) nanoflakes, considering multiple adsorption orientations.

Following the initial geometry optimization of all structures, three key adsorption configurations designated as positions a, b, and c were identified as the most energetically favorable interaction sites (see Fig. 1).

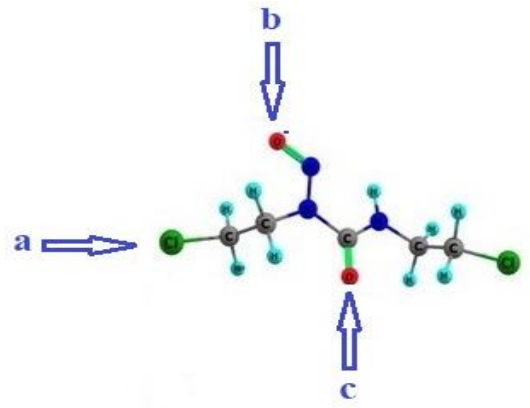

Fig. 1. 2D views of the Carmustine drug active position.

The nanoflakes are represented by the symbols B, G, and N, corresponding to BC_3, graphene, and NC_3, respectively. All adsorption models were optimized at the ωB97XD level of density functional theory (DFT) using the 6-31G(d,p) basis set. The optimized structures are depicted in Fig. 2 and S1. Structural analysis reveals that the shortest interaction distances between the Carmustine drug and the nanoflakes follow the trend: NC_3 < BC_3 < G. Specifically, in the Cm&NC_3 complexes, the shortest drug-surface distances for the most stable configurations were determined as follows: N-b (2.257 Å) < N-a (2.699 Å) < N-c (2.831 Å).

These findings suggest that the incorporation of nitrogen and boron into the graphene lattice significantly alters the electronic environment of the nanoflakes, leading to enhanced adsorption interactions. The observed reduction in drug-surface distance upon doping indicates stronger binding, which correlates with an increase in the adsorption energy (E_{ads}). This enhancement in adsorption strength suggests that NC_3 and BC_3 nanoflakes may serve as promising candidates for drug delivery and sensing applications due to their improved interaction capabilities with Carmustine.

The adsorption energies (E_{ads}) for all Carmustine-nanoflake complexes were calculated in both gaseous and aqueous phases using Eq. (1), with the results summarized in Table 1. A detailed analysis of the computed E_{ads} values reveals that the Carmustine (Cm) drug exhibits the strongest adsorption on NC_3 nanoflakes compared to BC_3 and graphene, suggesting that NC_3 serves as the most effective carrier for targeted drug delivery.

Among the adsorption configurations, the N-b position exhibits the highest adsorption energy (-33.44 kcal mol^{-1}), whereas the G-a position has the lowest adsorption energy (-20.26 kcal mol^{-1}), indicating that Carmustine binds most strongly at the N-b site on NC_3 and least strongly at the G-a site on graphene. A comparative evaluation of E_{ads} values in gaseous and aqueous phases demonstrates that all complexes maintain negative adsorption energies in both environments, confirming the exothermic and thermodynamically favorable nature of the adsorption process. However, the E_{ads} values in the aqueous phase are consistently lower than in the gas phase, indicating a weaker interaction due to solvation effects. The trend in adsorption strength across different nanoflakes and adsorption sites follows the order: N-b > N-a > N-c > BC_3-b > BC_3-a > BC_3-c > G-b = G-c > G-a. These findings highlight that the incorporation of nitrogen and boron atoms into the graphene framework in a 1:3 ratio significantly enhances the drug-nanoflake interaction. The stronger binding observed in NC_3 and BC_3 nanoflakes suggests their potential as efficient nanocarriers for the controlled and targeted delivery of Carmustine, improving its therapeutic efficacy in drug delivery applications.

The Recovery Time

The recovery time (τ) is exponentially proportional to E_{ads} and given by the following equation, called transition state theory

$$\tau = \upsilon^{-1}.\exp^{(-E_{ads}/kT)} \quad (\upsilon = 1\times10^{-12},\ k = 1.98\times10^{-3}, T = 298.15K)$$

[60].

The recovery times (τ) for all Carmustine-nanoflake complexes were calculated, and the corresponding values are presented in Table 1. A detailed analysis of the computed recovery times indicates that the N-b complex exhibits the highest τ value, signifying a prolonged interaction between the Carmustine drug and the NC_3 nanoflake. This suggests that the drug remains adsorbed on the NC_3 surface for an extended period, potentially enhancing its effectiveness as a drug carrier by ensuring sustained release.

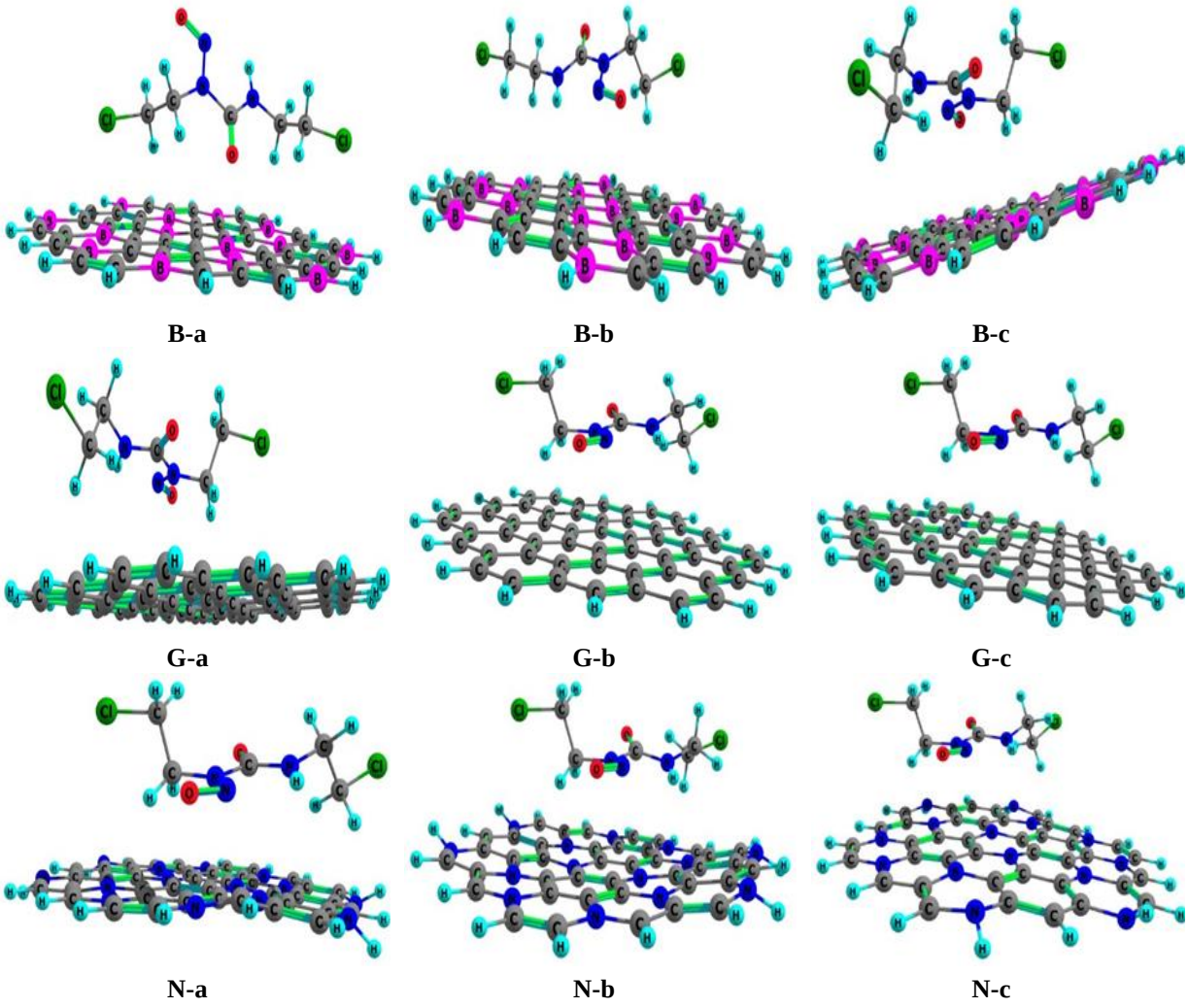

Fig. 2. The optimized structures of the interaction of Carmustine drug with Graphene, NC_3, and BC_3 nanoflakes.

Table 1. The Adsorption Energy, Enthalpy, and Gibbs Free Energy of Interaction of Carmustine Drug with Graphene, NC_3, BC_3 Nanoflakes in the Presence of Water Solvent

	$\Delta G_{(gas)}$ (kcal mol^{-1})	ΔH (kcal mol^{-1})	$E_{ads(gas)}$ (kcal mol^{-1})	$E_{ads(sol)}$ (kcal mol^{-1})	$\tau_{(gas)}$ (s)	$\tau_{(w)}$ (s)	$\Delta\Delta G_{(w)}$ (kcal mol^{-1})	$\Delta G_{(w)}$ (kcal mol^{-1})
B-a	-10.09	-18.20	-22.58	-21.57	1.08×10^{-2}	3.94×10^{-3}	2.59	-7.50
B-b	-10.10	-18.80	-21.97	-20.87	5.87×10^{-3}	1.95×10^{-3}	2.58	-7.52
B-c	-10.68	-19.31	-23.89	-21.98	4.01×10^{-2}	5.93×10^{-3}	2.00	-8.68
G-a	-13.80	-17.23	-20.26	-19.39	1.06×10^{-3}	4.45×10^{-4}	1.42	-12.38
G-b	-13.66	-18.23	-20.82	-20.09	1.86×10^{-3}	8.96×10^{-4}	1.56	-12.10
G-c	-13.66	-18.23	-20.82	-20.09	1.86×10^{-3}	8.96×10^{-4}	1.56	-12.10
N-a	-21.52	-20.59	-30.60	-26.17	3.29×10^{1}	3.92×10^{-1}	2.86	-18.66
N-b	-23.09	-22.64	-33.44	-27.26	5.63×10^{2}	1.16×10^{0}	4.29	-18.80
N-c	-21.40	-18.75	-28.24	-23.93	3.10×10^{0}	4.17×10^{-2}	2.98	-18.42

In contrast, the τ values for the Cm&G complexes are comparatively lower, indicating that the drug desorbs more readily from the graphene surface. This implies a weaker interaction, leading to a shorter retention time of the drug near the nanoflake. The observed variation in recovery times across different nanoflakes aligns with the adsorption energy (E_{ads}) trends, reinforcing the conclusion that NC_3 provides the most favorable environment for drug retention and controlled release, followed by BC_3, while graphene exhibits the weakest interaction.

These findings suggest that NC_3 and BC_3 nanoflakes could be promising candidates for drug delivery applications, where prolonged interaction and controlled release are desirable for enhanced therapeutic efficacy.

Thermodynamic Parameters and IR Spectrum

The enthalpy change (ΔH) and Gibbs free energy change (ΔG) for the adsorption process in the gas phase were calculated using Eqs. (2) and (3), with the corresponding results presented in Table 1 and illustrated in Fig. 3.

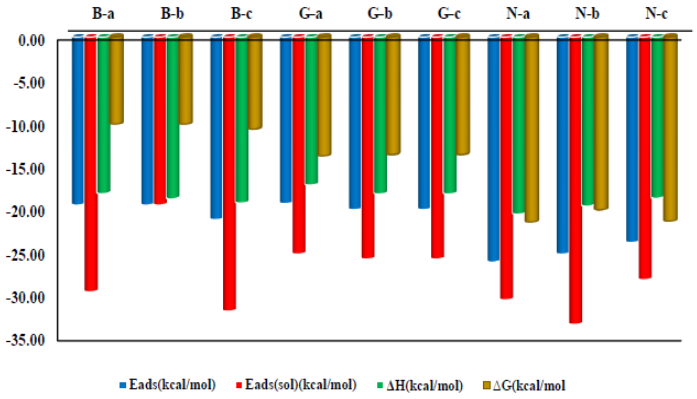

Fig. 3. The adsorption energies in gas and aqueous media, and thermodynamic parameters of the interaction of Carmustine drug with Graphene, NC3, and BC3 nanoflakes.

A detailed thermodynamic analysis reveals that both ΔH and ΔG are negative for all adsorption models, indicating that the adsorption process is exothermic and thermodynamically spontaneous. The negative ΔH values confirm that energy is released during the adsorption, enhancing the stability of the drug-nanoflake complexes. Meanwhile, the negative ΔG values suggest that the interaction between the Carmustine drug and the nanoflakes occurs without requiring external energy input, reinforcing the feasibility of the adsorption process under physiological conditions. Among the studied complexes, the Cm&NC_3 system exhibits the most negative thermodynamic parameters, signifying the strongest interaction between the Carmustine drug and NC_3 nanoflakes. This finding suggests that NC_3 nanoflakes are particularly effective as drug carriers, providing stable adsorption that may facilitate controlled and sustained drug delivery to target cells. Infrared (IR) spectral analysis reveals several key absorption features. The stretching of the N-H bond is observed in the range of 100 to 3750 cm^{-1}. A strong absorption band between 750 and 800 cm^{-1} corresponds to the stretching of the C=C bond in the Carmustine drug. The absorption in the 1200 to 1300 cm^{-1} range is attributed to the stretching of the C-N bond, while the 1000 to 1100 cm^{-1} range is associated with the stretching of the C-O bond. Additionally, the stretching of the C–Cl bond is evident in the frequency range of 550 to 800 cm^{-1}. These findings are in excellent agreement with previously reported values for the drug and nanoflakes [29].

Solvent Effects

To explore the solvent effects on the interaction between the Carmustine (Cm) drug and the graphene (G), BC_3, and NC_3 nanoflakes, the Polarizable Continuum Model (PCM) was employed. In this approach, the solvent (water) is modeled as a continuously polarizable dielectric medium, while the solute (drug-nanoflake complex) is treated as a non-polarizable entity [61-62]. This method allows for the implicit inclusion of solvation effects, providing a more realistic representation of the adsorption behavior in biological environments. To quantify these solvent effects, the solvation Gibbs free energies ($\Delta G_{(sol)}$) and the solvation-induced Gibbs free energy changes ($\Delta\Delta G_{(sol)}$) for the Cm&graphene, Cm&BC_3, and Cm&NC_3 complexes were computed using Eqs. (4) and (5). These calculations enable a comparative assessment of adsorption stability in aqueous and gaseous environments, shedding light on the role of solvent interactions in modulating the adsorption strength and thermodynamic feasibility of the drug-nanoflake complexes.

$$\Delta\Delta G_{(sol)} = \Delta G_{(sol)(Nano-CM)} - \Delta G_{(sol)(Nano)} - \Delta G_{(sol)(CM)} \quad (4)$$

$$\Delta G_{(sol)} = \Delta G_{(gas)} + \Delta\Delta G_{(sol)} \quad (5)$$

The calculated solvation-induced Gibbs free energy changes ($\Delta\Delta G_{(sol)}$) for all studied complexes are positive, indicating that solvation slightly reduces the adsorption stability compared to the gas phase. This suggests that interactions between the Carmustine drug and the nanoflakes are somewhat weaker in the aqueous phase due to competing solute-solvent interactions. However, the Gibbs free energy of solvation ($\Delta G_{(sol)}$) values for the Cm&G, Cm&BC_3, and Cm&NC_3 complexes are negative, confirming that the adsorption process remains thermodynamically spontaneous in water. This negative $\Delta G_{(sol)}$ signifies that despite the influence of solvation effects, the drug still preferentially adsorbs onto the nanoflake surfaces, making these materials viable candidates for drug delivery applications in physiological environments. Among the studied configurations, the absolute values of $\Delta G_{(sol)}$ for the N-a (-18.66 kcal mol^{-1}), N-b (-18.80 kcal mol^{-1}), and N-c (-18.42 kcal mol^{-1}) complexes are higher than those of other adsorption models (see Table 1). This trend indicates that the interaction between Carmustine and NC_3 nanoflakes is the most thermodynamically favorable and spontaneous in aqueous conditions. The stronger interaction observed in NC_3 compared to BC_3 and graphene suggests that NC_3 nanoflakes exhibit superior adsorption capability, making them promising candidates for efficient and stable drug delivery systems in biological environments.

HOMO-LUMO Orbitals and Quantum Descriptors

The highest occupied molecular orbital (HOMO) and the lowest unoccupied molecular orbital (LUMO) play a fundamental role in determining the electronic properties, chemical reactivity, and charge transfer characteristics of molecular systems.

These orbitals are particularly important for understanding molecular interactions, adsorption behavior, and electronic transitions in drug-nanoflake complexes. The HOMO and LUMO densities for all studied complexes were computed, and the results are visually represented in Figs. 4 and S3. A detailed analysis of their spatial distributions reveals that both orbitals exhibit significant localization on the surfaces of the nanoflakes. This preferential orbital localization indicates that the nanoflakes serve as active sites for electronic interactions, enhancing their ability to interact with electrophilic and nucleophilic species. The observed HOMO and LUMO distributions suggest that the nanoflakes facilitate efficient charge transfer between the Carmustine drug and the substrate, which is a key factor in adsorption stability and electronic coupling. This finding further supports the potential of NC_3 and BC_3 nanoflakes as promising candidates for drug delivery and sensing applications, where strong electronic interactions are advantageous.

The density of states (DOS) is a fundamental concept in solid-state physics and materials science, describing the number of accessible electronic states per unit energy interval. DOS analysis provides critical insights into the electronic band structure, charge transport properties, and optical activity of materials, making it an essential tool in the design of semiconductors, nanomaterials, and electronic devices. In this study, the DOS profiles for the Cm&G, Cm&BC_3, and Cm&NC_3 complexes were computed using Gauss Sum software [63] over an energy range of -20 to 15 eV, and the results are illustrated in Figs. 4 and S4. The HOMO and LUMO regions exhibit distinct peak distributions, with the number of peaks observed for the B-b, G-b, and N-b configurations being (14, 21), (16, 18), and (17, 19), respectively. A comparative analysis of the DOS peak intensities and heights reveals a decreasing trend in the order: Cm&G > Cm&BC_3 > Cm&NC_3. This gradual reduction in peak intensity with the substitution of B and N atoms suggests a decrease in the overall electronic density of states, leading to a reduction in the optical activity of the complexes. The observed trend indicates that the incorporation of heteroatoms (B, N) in graphene-based nanoflakes alters the electronic structure, potentially tuning their electronic and optoelectronic properties for applications in drug delivery, biosensing, and nanoelectronics.

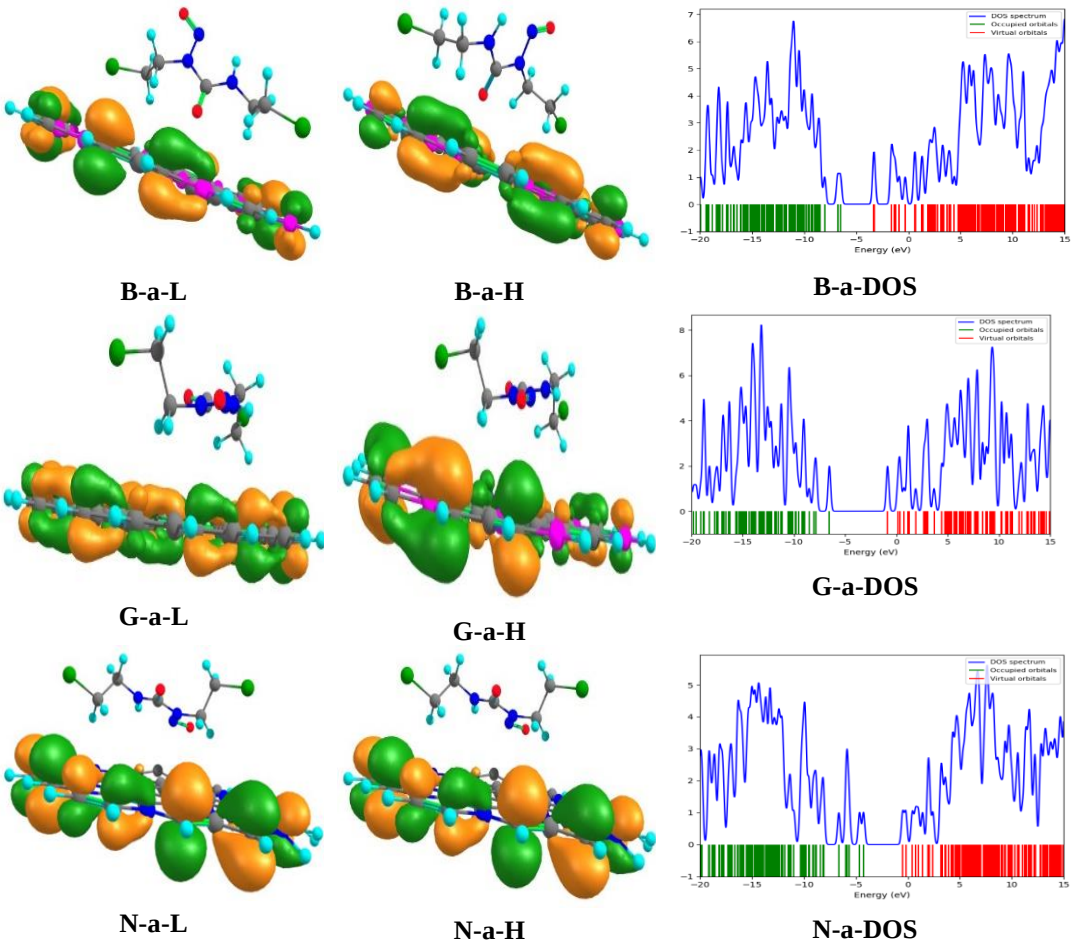

Fig. 4. HOMO and LUMO orbitals and DOS plots the interaction of Carmustine drug with Graphene, NC_3, and BC_3 nanoflakes in the (a) position.

The electronic properties of the studied complexes were evaluated using key quantum chemical descriptors, including the energy gap ($E_{gap} = E_{LUMO} - E_{HOMO}$), chemical hardness ($\eta = (E_{LUMO} - E_{HOMO})/2$), and chemical potential ($\mu = (E_{HOMO} + E_{LUMO})/2$) [64] were calculated from the HOMO and LUMO energies. A higher energy gap (E_{gap}) and chemical hardness (η) generally indicate greater chemical stability and lower reactivity, whereas a smaller gap implies enhanced charge transfer capability and greater reactivity, which are crucial for applications in drug delivery and sensing. According to the results summarized in Table 2, the E_{gap} and η values for all studied complexes fall within the ranges of 3.13 to 5.68 eV and 1.56 to 2.84 eV, respectively. The lowest E_{gap} and η values are observed for the B-b adsorption model, indicating enhanced conductivity and reactivity, while the highest values are found in the G-c and G-b models, reflecting greater stability and lower reactivity. The observed trend in E_{gap} and η follows the order: Cm&BC < Cm&NC < Cm&G. This progressive reduction in energy gap and chemical hardness upon substituting B and N atoms into the graphene lattice suggests that BC_3 and NC_3 nanoflakes enhance the electronic conductivity and chemical reactivity of the system. Consequently, these materials exhibit superior potential for use in drug tracking and sensing applications, where stronger electronic interactions are desirable. Additionally, the chemical potential (μ) of the Cm&BC_3 complex is higher compared to the Cm&NC_3 and Cm&G complexes, indicating that the BC_3 nanoflake provides a more stable adsorption platform for the Carmustine drug. This further supports the potential of BC_3-based nanomaterials in targeted drug delivery and biomedical applications.

Table 2. Quantum Descriptors (HOMO, LUMO Energies, Gap Energy, eElectrical Potential, and Chemical Hardness) of the Interaction of Carmustine Drug with Graphene, NC_3, BC_3 Nanoflakes

	E_{LUMO} eV	E_{HOMO} eV	E_{gap} eV	η eV	μ eV
B-a	-3.33	-6.52	3.18	1.59	-4.93
B-b	-3.55	-6.98	3.13	1.56	-5.26
B-c	-3.47	-6.62	3.15	1.57	-5.04
G-a	-0.87	-6.53	5.66	2.83	-3.70
G-b	-0.88	-6.56	5.68	2.84	-3.72
G-c	-0.88	-6.56	5.68	2.84	-3.72
N-a	-0.49	-4.26	3.77	1.88	-2.37
N-b	-0.40	-4.20	3.80	1.90	-2.30
N-c	-0.41	-4.21	3.79	1.89	-2.31

Table 3. The Topological Parameters of AIM Theory and ELF and LOL Values of the Interaction of Carmustine Drug with Graphene, NC_3, BC_3 Nanoflakes

	ρ	H(r)	V(r)	$\nabla^2\rho$	ELF
B-a	0.0139	0.0001	-0.0110	0.0432	0.0427
B-b	0.0091	0.0003	-0.0063	0.0279	0.0268
B-c	0.0165	0.0045	-0.0153	0.0977	0.0233
G-a	0.0193	0.0027	-0.0149	0.0815	0.0485
G-b	0.0070	0.0013	-0.0035	0.0247	0.0231
G-c	0.0074	0.0013	-0.0039	0.0265	0.0229
N-a	0.4244	0.0467	-0.0468	0.0180	0.0999
N-b	0.0072	0.0010	-0.0046	0.0274	0.0179
N-c	0.0131	0.0007	-0.0092	0.0435	0.0411

AIM Topological Parameters

The Atoms in Molecules (AIM) theory, also known as Quantum Chemical Topology (QCT), offers a framework for analyzing the electron density topology in molecular systems. Developed by Richard Bader, this theory utilizes topological parameters to elucidate the nature of chemical bonds and interactions. Key to this theory are critical points (CPs), where the gradient of electron density is zero [54]. At these critical points, particularly Bond Critical Points (BCPs), the electron density (ρ) provides insights into bond strength and type. The Laplacian of the electron density ($\nabla^2\rho$) indicates whether the electron density is locally concentrated ($\nabla^2\rho < 0$) or depleted ($\nabla^2\rho > 0$), thus helping to characterize the nature of chemical interactions. Additionally, parameters such as potential energy density (V_{BCP}) and total energy density (H_{BCP}) at critical points offer information on bond energetics. These topological parameters are valuable for analyzing chemical bonding, molecular structure, and reactivity, especially in weak interactions such as hydrogen bonds and van der Waals forces, which may not be adequately described by traditional bonding models. In this study, electron densities (ρ), Laplacian of electron densities ($\nabla^2\rho$), and total electron energy (H_{BCP}) at BCPs for the Cm&G, Cm&BC_3, and Cm&NC_3 complexes were computed using Multiwfn software [65]. The results are presented in Table 3. According to Bader's theory, if $\nabla^2\rho$ and H_{BCP} are both less than zero, the bond is characterized as covalent. Conversely, if $\nabla^2\rho$ and H_{BCP} are both greater than zero, the bond is considered electrostatic. If $\nabla^2\rho$ is less than zero and H_{BCP} is greater than zero, the bond is partially covalent. The results presented in Table 3 indicate that H_{BCP} and $\nabla^2\rho$ for the Cm&G, Cm&BC_3, and Cm&NC_3 complexes are all greater than zero, suggesting that the interactions between the Cm-drug and the nanoflakes are predominantly non-covalent.

ELF Analysis

The Electron Localization Function (ELF) serves as a powerful quantum chemical tool for examining and visualizing the spatial distribution of electrons within molecules and solid-state systems. ELF provides complementary insights into chemical bonding and electron distribution alongside conventional approaches such as molecular orbital and electron density analyses. Conceptually, ELF quantifies the likelihood of finding an electron in the vicinity of a reference electron at a specific spatial point, with values ranging from 0 to 1. Values approaching 1 indicate strong electron localization, typical of covalent bonds and lone electron pairs. Values near 0.5 signify delocalized electrons, as commonly observed in metallic or weakly bonded systems, whereas values close to 0 correspond to regions of very low electron density. In the present study, as summarized in Table 3, the ELF values for all examined Carmustine–nanoflake complexes are below 0.5, highlighting the predominance of delocalized electrons. This observation suggests that the interactions between the Carmustine drug and the nanoflakes are primarily electrostatic in nature. The ELF topological maps, depicted in Fig. 5, use red to indicate regions of high electron density, blue for areas with very low electron density, and green for regions of intermediate electron density. Examination of these plots reveals that electron density between the Carmustine molecule and the nanoflakes is relatively low compared to other regions, further supporting the non-covalent character of the interaction.

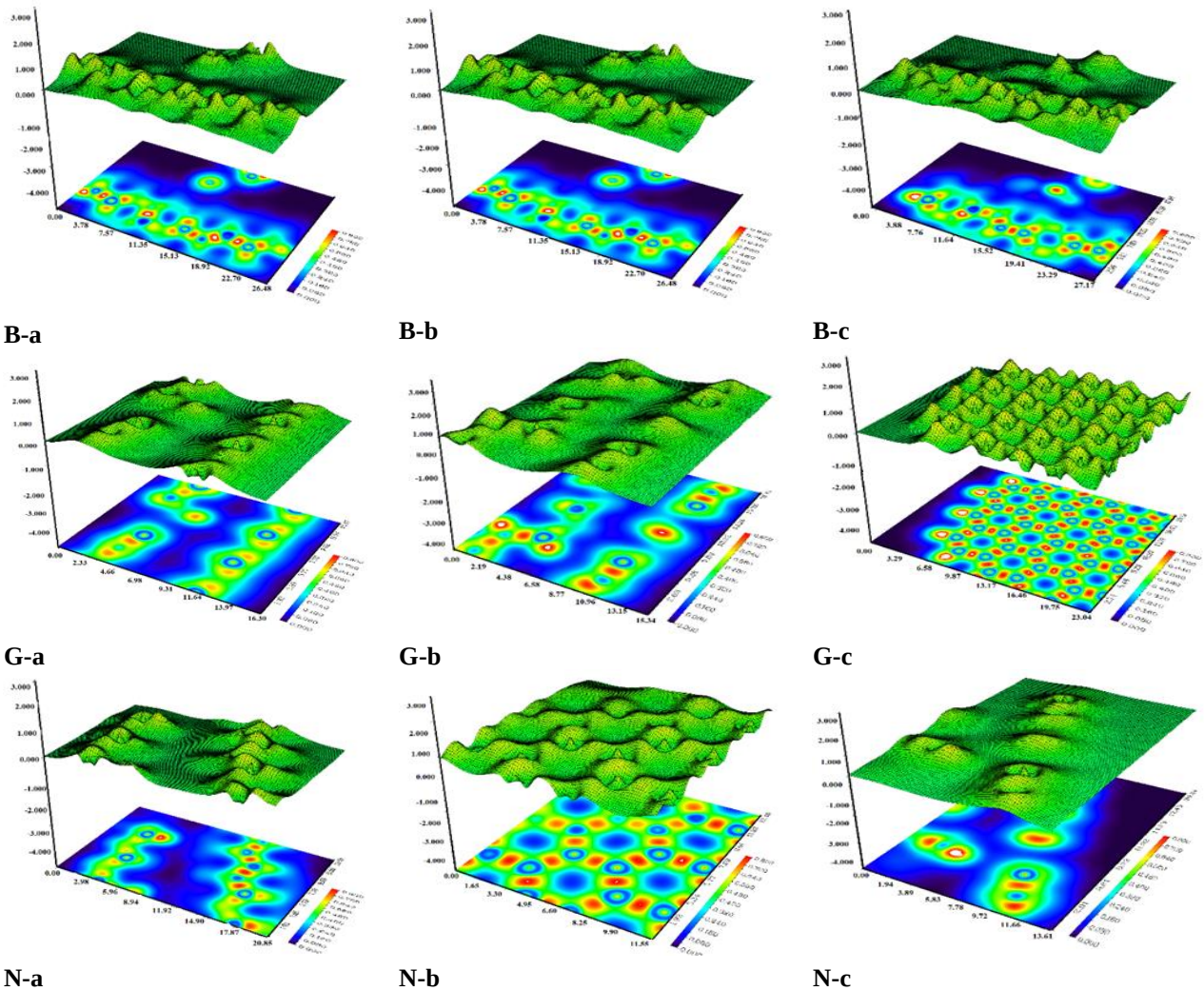

Fig. 5. ELF plots of the interaction of Carmustine drug with Graphene, NC_3, and BC_3 nanoflakes.

Specifically, the highest electron localization is observed on the surface of the Carmustine molecule, whereas the nanoflakes (BC_3, G, and NC_3) exhibit lower electron density at their surfaces. This trend confirms the electrostatic dominance in the bonding interactions. Among the studied complexes, the electron distribution between Carmustine and BC_3 or NC_3 nanoflakes is more pronounced than in the other systems, suggesting stronger noncovalent interactions and indicating the potential of these nanoflakes as effective platforms for targeted drug delivery. Regarding the visualization, the Carmustine molecule adopts an approximately planar geometry upon optimization, and the ELF cross-sectional planes in Fig. 5 were chosen to intersect the primary interaction regions between the drug and nanoflake surfaces, specifically along planes passing through atoms involved in the shortest intermolecular distances. This approach enables a clear depiction of electron localization in the interface regions where noncovalent interactions occur. As confirmed in Table 3 and Section 3.6, the sub-0.5 ELF values reinforce the delocalized nature of electrons and the electrostatic character of the interactions. In the maps, red areas correspond primarily to electron-rich regions on the drug, while blue and green regions highlight areas of low electron density on the nanoflakes. These refinements in figure captions and discussion improve clarity and accurately describe the orientation of the ELF planes. Overall, these results suggest that BC_3 and NC_3 nanoflakes exhibit favorable electron interaction patterns, making them promising candidates for the targeted delivery of Carmustine

RDG Plots Analyses

The Reduced density gradient (RDG) is a fundamental concept in density functional theory (DFT) and is particularly useful for analyzing non-covalent interactions in molecular systems. The reduced density gradient is a dimensionless quantity derived from the electron density ($\rho_{(r)}$) and its gradient ($\nabla\rho_{(r)}$). It's defined as:

$$RDG(r) = \frac{1}{2(3\pi^2)^{1/3}} \frac{|\nabla\rho(r)|}{\rho(r)^{4/3}} \quad (6)$$

Where $\rho_{(r)}$ represents the electron density and $\nabla\rho_{(r)}$ denotes the gradient of the electron density. RDG analysis is a key component of the Non-Covalent Interaction (NCI) index, which helps identify and characterize weak interactions such as hydrogen bonds, van der Waals forces, and steric repulsion. RDG is typically plotted against the sign of the second eigenvalue of the electron density Hessian matrix (λ_2). This NCI plot helps reveal different types of interactions: hydrogen bonds are associated with sharp peaks at low RDG values and negative λ_2 (indicated by blue regions where $\lambda_2 < 0$); van der Waals interactions correspond to low RDG values and near-zero λ_2 (green regions where $\lambda_2 \approx 0$); and steric repulsion is indicated by peaks at positive λ_2 values (red regions where $\lambda 2 > 0$) [55]. The RDG scatter and isosurface plots shown in Figure 6 indicate that the highest RDG densities are concentrated in regions with $\lambda_2 < 0$ or ~ 0. This suggests that the primary nature of the interactions between Carmustine and the BC_3, graphene (G), and NC_3 nanoflakes is either electrostatic or hydrogen bonding. Furthermore, the RDG density is notably highest in the N-b and B-c models compared to other complexes, indicating stronger electrostatic interactions between the Cm-drug and the BC_3 and NC_3 nanoflakes. These findings are consistent with the results obtained from AIM and ELF analyses, reinforcing the nature and strength of the interactions observed.

UV-Visible Spectroscopy

UV-visible spectroscopy is a powerful analytical technique used to measure the absorption or reflection of ultraviolet (UV) and visible light by a sample. This technique provides insights into the electronic transitions within molecules, as well as the presence of conjugated systems or chromophores that are capable of absorbing light in the UV-visible region. The resulting UV-visible spectrum is a plot of absorbance (or transmittance) against the wavelength (or frequency) of the incident light. It typically shows one or more absorption peaks that correspond to specific electronic transitions, which can be associated with the movement of electrons between molecular orbitals, such as transitions from the ground state to excited states. UV-visible spectroscopy is indispensable for studying the electronic structure, reactivity, and chemical mechanisms of compounds. It plays a critical role in various fields such as organic synthesis, catalysis, materials science, and biochemistry [58-59].

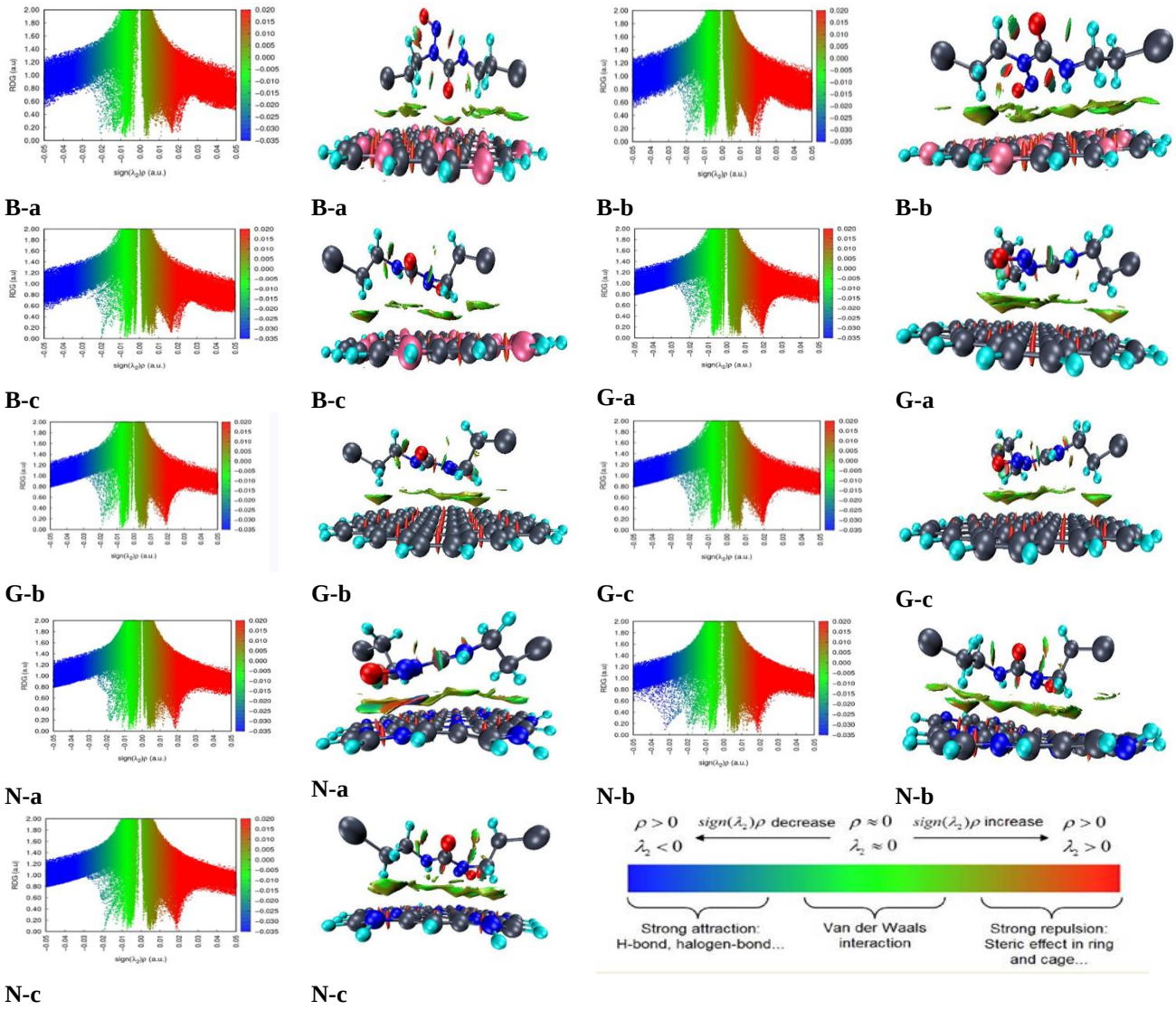

Fig. 6. RDG scatter plots and isosurface of the interaction of Carmustine drug with Graphene, NC_3, and BC_3 nanoflakes.

The spectral features, such as the oscillator strength (*f*) and maximum absorption wavelength (λ_{max}), provide crucial information about the electronic properties of molecules, including their conjugation and potential for light absorption, which is important for applications like drug delivery, sensing, and optoelectronics. In this study, the UV-visible spectra and electronic transition states of the complexes under investigation are presented in Figs. 7 and S5, with the transition state data further detailed in Table S1. The oscillator strength (*f*) and maximum wavelength (λ_{max}) for these complexes range from 0.1312 to 1.4515 and 344.16 to 1061.57 nm, respectively. These values indicate the strength and position of the absorption peaks, providing insights into the electronic properties of the complexes. As shown in Fig. 7, the B-a, B-b, and B-c models exhibit absorption peaks at wavelengths of 1042.76 nm (*f* = 0.334), 1061.57 nm (*f* = 0.318), and 1049.11 nm (*f* = 0.202), respectively, corresponding to the electronic transition from $S_0 \rightarrow S_2$. These results suggest that the substitution of B and N atoms in the nanoflake structures leads to absorption at longer wavelengths, shifting the absorption to the visible region compared to the absorption peaks observed for graphene.

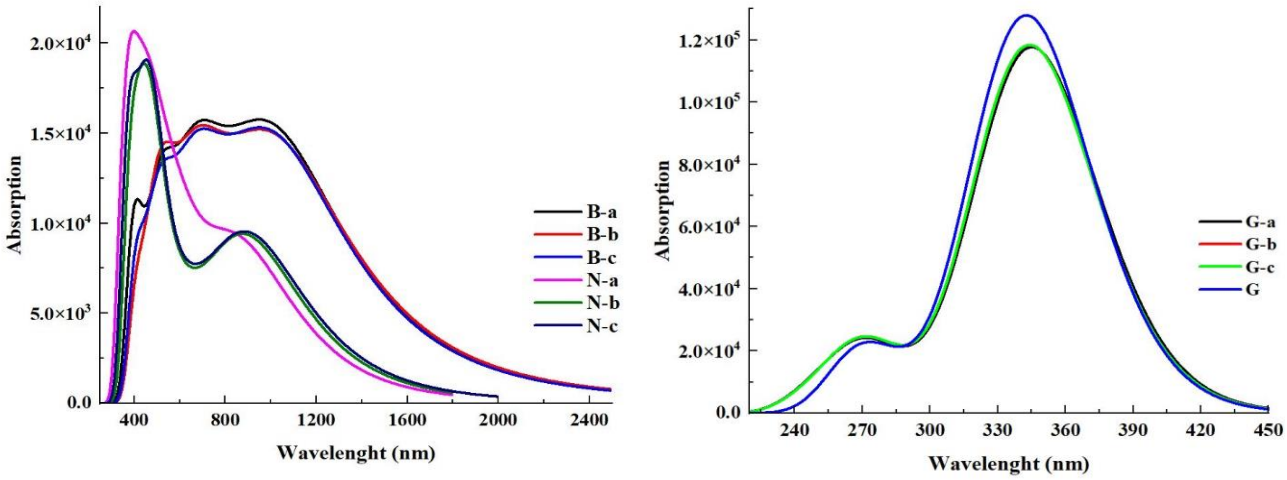

Fig. 7. UV-visible spectrum of the interaction of Carmustine drug with Graphene, NC_3, and BC_3 nanoflakes.

This indicates that doping the graphene structure with B and N atoms can tune the material's electronic properties, making it more suitable for applications in the visible light spectrum. Furthermore, the absorption intensity varies significantly among the different models, which makes UV-visible spectroscopy an effective tool for distinguishing between the different drug-nanoflake complexes. The distinct absorption characteristics observed for each complex also suggest differences in electronic interactions between the drug and the nanoflake surfaces. This differential absorption is valuable for identifying the interaction strength and can be used to monitor drug interactions in biological systems. When combined with the study of non-linear optical (NLO) properties, UV-visible spectroscopy emerges as a powerful tool for tracking the dynamics of drug delivery and targeted drug interactions within biological environments, as well as providing insights into the biocompatibility and efficiency of drug delivery systems.

CONCLUSIONS

This study provides a comprehensive investigation into the interaction of the Carmustine drug with BC_3, NC_3, and G nanoflakes, utilizing density functional theory (DFT) at the ωB97XD/6-31G(d,p) level of theory. The structural optimization results indicate that the shortest interaction distances between Carmustine and the nanoflakes follow the order: $NC_3 < BC_3 < G$, demonstrating the strong affinity of NC_3 nanoflakes for the drug. The adsorption energies (E_{ads}) for all complexes, in both the gas and aqueous phases, are negative, signifying exothermic adsorption processes. Among the studied models, the N-b configuration exhibits the highest adsorption energy (-33.44 kcal mol^{-1}), while the G-a configuration shows the lowest (-20.26 kcal mol^{-1}), highlighting the superior binding strength of NC_3. Notably, the N-b model also demonstrates the longest recovery time (τ), further emphasizing its stability. Thermodynamic analyses, including Gibbs free energy changes (ΔG), indicate that the adsorption processes are spontaneous in both the gas and solvent phases, as all ΔG values are negative. Furthermore, the energy gap and chemical hardness analyses reveal that the B-b model has the lowest values, suggesting enhanced electronic interactions, while the G-c and G-b models exhibit the highest values, indicating reduced reactivity. These findings underscore the superior potential of BC_3 and NC_3 nanoflakes in the development of sensitive sensors and targeted drug delivery systems. Advanced quantum descriptors, such as Atoms in Molecules (AIM), Electron Localization Function (ELF), and Reduced Density Gradient (RDG) analyses, demonstrate that the interactions between Carmustine and the BC_3 and NC_3 nanoflakes are predominantly non-covalent and electrostatic. These analyses also confirm the enhanced electron distribution in the BC_3 and NC_3 complexes, further validating their

suitability for drug-targeting applications. UV-visible (UV-Vis) spectroscopy analyses reveal significant shifts in the maximum absorption wavelength (λ_{max}) for the BC_3 and NC_3 complexes compared to graphene, offering a robust mechanism for drug tracking in biological systems. In conclusion, BC_3 and NC_3 nanoflakes emerge as promising candidates for the targeted delivery of Carmustine and the development of sensitive drug-tracking sensors, presenting substantial advancements in nanomedicine and therapeutic monitoring technologies.

Supplementary Data

Table S1 and Figures S1- S5 are given in the supplementary data.

ACKNOWLEDGMENTS

The authors express their sincere gratitude to Malayer University for providing the necessary facilities and support for this research.

REFERENCES

[1] Geim, A. K.; Novoselov, K. S., The rise of graphene. *Nature Mater*. **2007**, *6*(3), 183-191. https://doi.org/10.1038/nmat1849.

[2] Liu, Z.; Robinson, J.T.; Sun, X.; Dai, H.; P. E., Gylated Nano graphene oxide for delivery of water-insoluble cancer drugs. *J. Am. Chem. Soc*. **2008**, *130*(33) 10876-10877. https://doi.org/10.1021/ja803688x.

[3] Yang, K.; Feng, L.; Shi, X.; Liu, Z., Nano-graphene in biomedicine: theranostic applications. *Chem. Soc. Rev.* **2013**, *42*(2), 530-547. https://doi.org/10.1039/C2CS35342C.

[4] Shen, H.; Zhang. L.; Liu, M.; Zhang, Z., Biomedical applications of graphene. *Theranostic*. **2012**, *2*(3), 283-294. DOI: 10.7150/thno.3642.

[5] Ahmed, F. Z.; Ahmad, A. A.; Kharazian, B., A Molecular Dynamics Study of the Interaction Between Graphene as a Carrier and Gemcitabine as a Chemotherapy. *Zanco J. Pure and Applied Sci*. **2023**, *35*(1), 23-29. https://doi.org/10.21271/ZJPAS.35.1.3

[6] Ibrahim, M. A. A.; Hamad, M. H. A.; Mahmoud, A. H. M.; Michener, G. A. H.; Sayed, S. R. M.; Abd El-Rahman, M. K.; Sidhom, P. A.; Dabbish, E.; Shoeib, T., On the Use of Graphene Nanoflakes for Drug Delivery: A Case Study of Cisplatin and Some of Its Analogs. *Pharmaceutics.* **2023** *15*(6), 1640. https://doi.org/10.3390/pharmaceutics15061640.

[7] Al-Qargholi, B.; Tabassum, S.; Abbass, R.; Al-Saidi, D. N.; Gatea, M. A.; Fazaa, A. H.; Saraswat, S. K.; Petrosian, S.; Li, W., Nanoflakes (CC-BC3-C3N) as a carrier for favipiravir drug: A density functional theory study, *Inorganic Chem. Comm.* **2023**, *150*, 110475. https://doi.org/10.1016/j.inoche.2023.110475.

[8] Gong, P.; Zhou, Y.; Li, H.; Zhang, J.; Wu, Y.; Zheng, P.; Jiang, Y., Theoretical Study on the Aggregation and Adsorption Behaviors of Anticancer Drug Molecules on Graphene/Graphene Oxide Surface. *Molecules*, **2022**, *27*, 6742. https://doi.org/10.3390/molecules27196742.

[9] Zaboli, A.; Raissi, H.; Farzad, F.; Hashemzadeh, H.; Fallahi, F.; Cation-pi interaction: A strategy for enhancing the performance of graphene-based drug delivery systems, *Inorganic Chem. Comm*. **2022**, *141*, 109542. https://doi.org/10.1016/j.inoche.2022.109542.

[10] Del Castillo, R. M.; Ramos, E.; Martínez, A., Interaction of graphene with antipsychotic drugs: Is there any charge transfer process? *J. Comput. Chem*. **2021**, *42*(1), 60-65. https://doi.org/10.1002/jcc.26433.

[11] Xu, S.; Wang, T.; Liu, G.; Cao, Z.; Frank, L.A.; Jiang, S.; Zhang, C.; Li, Z.; Krasitskaya, V. V.; Li, Q.; Sha, Y.; Zhang, X.; Liu, H.; Wang, J., Analysis of interactions between proteins and small-molecule drugs by a biosensor based on a graphene field-effect transistor, *Sens. Actu. B: Chem.* **2021**, *326*, 128991. https://doi.org/10.1016/j.snb.2020.128991.

[12] Wang, H.; Wu, H.; Yang, J.; C3N: a two-dimensional semiconductor material with high stiffness, superior stability, and bending Poisson's effect. *arXiv preprint arXiv.* **2017**, 1703.08754. https://doi.org/10.48550/arXiv.1703.08754.

[13] Poor Heravi, M. R.; Azizi, B.; Mahmood, E. A.; Ebadi, A. G.; Ansari, M. J.; Soleimani-Amiri, S., Molecular simulation of the paracetamol drug interaction with Pt-decorated BC_3 graphene-like nanosheet, *Mol. Simul*. **2022,** *48*(8), 1-9. https://doi.org/10.1080/08927022.2022.2030861.

[14] Ibrahim, M. A. A.; Hamad, M.; Mahmoud, A. H. M.; Mekhemer, G. A. H.; Sayed, S. R. M.; Abd Elrahman, M.; Sidhom, P. A.; Dabbish, E.; Shoeib, T., On

the Use of Graphene Nanoflakes for Drug Delivery: A Case Study of Cisplatin and Some of Its Analogs, *Pharmaceutics*. **2023**, *15*(6), 1640. https://doi.org/10.3390/pharmaceutics15061640.

[15] Zeng, R.; Cai, L.; Perez-Aguilar, J. M.; Gu, Z.; Liu, X., Robust Mechanical Destruction to the Cell Membrane of Carbon Nitride Polyaniline (C3N): A Molecular Dynamics Simulation Study, *J. Chem. Inf. Model*. **2023**, *63*(13), 4170-4179. https://doi.org/10.1021/acs.jcim.3c00570.

[16] Akter Bithe, S.; Hasan, M.; Afrin Oishi, A.; Dhali, P.; Roy, D., To understand the miglitol adsorption behavior on BC3, BN, and GNS nanoflakes using DFT and QTAIM analysis for drug delivery applications, *Phys. Sci*. **2023**, *98*, 075010. DOI: 10.1088/1402-4896/acdccb.

[17] Carmustine. In NCI Drug Dictionary. National Cancer Institute. Retrieved from https://www.cancer.gov/publications/dictionaries/cancer-drug/def/carmustine, **2020**.

[18] Saikia, J.; Devi, T. G.; Karlo, T., Raman spectroscopy, AIM analysis, drug-likeness and molecular docking study of the hydrogen-bonded complex of Carmustine with Melatonin, *Mater. Today: Proc*. **2022**, *65*, 2875-2882. https://doi.org/10.1016/j.matpr.2022.06.433Get rights and content.

[19] Türker, L., Interaction of Carmustine Tautomers with Adenine - DFT Study, *J. Chem. Sci*. **2020**, *5*(1), 63-76. https://doi.org/10.34198/ejcs.5121.6376.

[20] Khorram, R.; Raissi, H.; Shahabi, M., Analysis of the structures, energetics, and vibrational frequencies for the hydrogen-bonded interaction of nucleic acid bases with Carmustine pharmaceutical agent: a detailed computational approach, *Struct. Chem*., **2018** *29*, 1165-1174. https://doi.org/10.1007/s11224-018-1102-8.

[21] Mortazavifar, A.; Raissi, H.; Akbari, A., DFT and MD investigations on the functionalized boron nitride nanotube as an effective drug delivery carrier for Carmustine anticancer drug, *J. Mole. Liq*. **2019**, *276*, 577-587. https://doi.org/10.1016/j.molliq.2018.12.028.

[22] Saharan, R.; Paliwal, S. K.; Tiwari, A.; Tiwari, V.; Singh, R.; Beniwal, S. K.; Dahiya, P., Sagadevan, S.; Exploring graphene and its potential in the delivery of drugs and biomolecules, *J. Drug Delivery Sci. Tech*. **2023**, *84*, 104446. https://doi.org/10.1016/j.jddst.2023.104446.

[23] Rostamian, R.; Amiri, N.; Behnejad, H., How does graphene nanosheet affect the pharmaceutical adsorption? A comprehensive insight from molecular dynamics simulation, quantum mechanics and experimental study, *J. Mole. Liq*. **2018**, 269, 29-37. https://doi.org/10.1016/j.molliq.2018.07.102.

[24] Khorram, R.; Raissi, H.; Morsali, A.; Shahabi, M., The computational study of the γ-Fe_2O_3 nanoparticle as Carmustine drug delivery system: DFT approach, *J. Biomol. Strut. Dyne*, **2019**, *37*, 454-464. https://doi.org/10.1080/07391102.2018.1429312.

[25] Khorram, R.; Raissi, H.; Morsali, A., Assessment of solvent effects on the interaction of Carmustine drug with the pristine and COOH-functionalized single-walled carbon nanotubes: A DFT perspective, *J. Mol. Liq*. **2017**, *240*, 87-97. https://doi.org/10.1016/j.molliq.2017.05.035.

[26] Soleymanabadi, H.; Karimkhani, M.; Taghva Manesh, A., The new type of heteroborospherene as a potential promising high drug-loading capacity for carmustine anticancer drug: Theoretical perspectives, *Comp. Theo. Chem.* **2024**, *1238*, 114741. https://doi.org/10.1016/j.comptc.2024.114741

[27] Wolski, P.; Narkiewicz-Michalek, J.; Panczyk, M.; Pastorin, G.; Panczyk, T., Molecular Dynamics Modeling of the Encapsulation and De-encapsulation of the Carmustine Anticancer Drug in the Inner Volume of a Carbon Nanotube, *J. Phys. Chem. C*, **2017**, *121*(34), 18922-18934. https://doi.org/10.1021/acs.jpcc.7b05229.

[28] Hoelm, M.; Porwański, S.; Jóźwiak, P.; Krześlak, A., Combined Theoretical and Experimental Investigations: Design, Synthesis, Characterization, and *In Vitro* Cytotoxic Activity Assessment of a Complex of a Novel Ureacellobiose Drug Carrier with the Anticancer Drug Carmustine, *Molecules*. **2024**, *29*(14), 3359. https://doi.org/10.3390/molecules29143359.

[29] Yi, S.; Yang, F.; Jie, C.; Zhang, G., A novel strategy to the formulation of carmustine and bioactive nanoparticles co-loaded PLGA biocomposite spheres for targeting drug delivery to glioma treatment and nursing care, Artificial Cells, Nanomed. *Biotech. Inter. J*. **2019**, *47*, 3438-3447. https://doi.org/10.1080/21691401.2019.1652628.

[30] Khanizadeh, A.; Ghaemi, A.; Pourmadadi, M.; Javadi, S.; Rahdar, A.; Yazdian, F.; Ghazy, E.; Pandey, S., Advancing cancer therapy: Unveiling the cutting-edge potential of carmustine nanocarriers for targeted treatment, *J. Drug Delivery Sci. Techno*. **2024**, *99*, 105943. https://doi.org/10.1016/j.jddst.2024.105943.

[31] Majumder, R.; Karmakar, S.; Mishra, S.; Mallick, A. B.; Mukhopadhyay, C. D., Functionalized Carbon Nano-Onions as a Smart Drug Delivery System for the Poorly Soluble Drug Carmustine for the Management of Glioblastoma, ACS. *Appl. Bio Mater*. **2024**, *7*(1), 154-167. https://doi.org/10.1021/acsabm.3c00688.

[32] Rahimi, R.; Solimannejad, M., *In silico* study of B_3O_3 nanosheet as a disposable platform for sensing and delivery of carmustine anticancer drug, *J. Drug Delivery Sci. Techno*. **2023**, *87*, 104828. https://doi.org/10.1016/j.jddst.2023.104828.

[33] Kamel, M.; Mohammadi, M.; Mohammadifard, K.; Mahmood, E. A.; Poor Heravi, M. R.; Heshmati, A.; Hossaini, Z., Comprehensive theoretical prediction of the stability and electronic properties of hydroxyurea and carmustine drugs on pristine and Chitosan-functionalized graphitic carbon nitride in vacuum and aqueous environment, *Vacuum*, **2023**, *207*, 111565. https://doi.org/10.1016/j.vacuum.2022.111565.

[34] Bin Iqbal, A. J.; Shahriar, R.; Zubair, A., First-principles study of a SiC nanosheet as an effective material for nitrosourea and carmustine anti-cancer drug delivery, *Nanoscale Adv*. **2024**, *6*, 2968-2979. DOI: 10.1039/D4NA00050A.

[35] Amiri Dolatabad, A.; Salehpour, M.; Saadati, Z., Hexa-peri-hexabenzocoronene as a vector sensing and delivery of Carmustine anticancer drug: A density functional theory study, *J. Mol. Liq.* **2024**, *407*, 125206. https://doi.org/10.1016/j.molliq.2024.125206.

[36] Begum, S. S.; Das, D.; Kishor Gour, N.; Chandra Deka, R., Computational modeling of nanotube delivery of the anti-cancer drug into glutathione reductase enzyme, *Sci. Rep*. **2021**, *11*, 4950. https://doi.org/10.1038/s41598-021-84006-1.

[37] Begum, S. S.; Kishor Gour, N.; Sonavane, U.; Kumar Ray, S.; Chandra Deka, R., Computational studies of anti-cancer drug-mediated by graphene and reaction mechanism of drug-generated alkyl radical with guanine, *J. Mol. Struc*. **2019**, *1196*, 527-535. https://doi.org/10.1016/j.molstruc.2019.06.101.

[38] Saikia, J.; Devi, T. G.; Karlo, T., Study of the molecular interaction between hormone and anti-cancer drug using DFT and vibrational spectroscopic methods, *J. Mol. Struc*. **2022**, *1250*, 131889. https://doi.org/10.1016/j.molstruc.2021.131889

[39] Xiao, J.; Li, Y.; Wang, Y.; Wang, X.; Zhang, W.; Liu, K., Study on the effect of superparamagnetic γ-Fe_2O_3 combined with carmustine on cervical cancer, *Mate. Exp*. **2020**, *10*(8), 1213-1217. https://doi.org/10.1166/mex.2020.1753.

[40] Rezaei-Sameti, M.; Torabi, H., Assessment of the Capability and Potential of Pristine, Sc-, Ti-, and Ni-Doped C24 Nanocages to Delivery and Sensor Property of Prothionamide Drug: Insight of DFT, TD-DFT Computational Methods, *J. Comput. Biophys. Chem*. **2023**, *22*, 1-18. https://doi.org/10.1142/S2737416523500266.

[41] Rezaei-Sameti, M.; Rezaei, A., A computational assessment of the interaction of 5Fluorouracil (5FU) drug connected to $B_{12}P_{12}$ and $ScB_{11}P_{12}$ nanocages with adenine nucleobase: DFT, AIM, TD-DFT study, *Struc. Chem*. **2023**, *35*(1), 1-14. https://doi.org/10.1007/s11224-023-02141-z.

[42] Rezaei-Sameti, M.; Barandisheh Naghibi, M., A quantum assessment of the interaction between $Si_{12}C_{12}$, $BSi_{11}C_{12}$, $BSi_{12}C_{11}$, $NSi_{11}C_{12}$ and $NSi_{12}C_{11}$ nanocages with Glycine amino acid: A DFT, TD-DFT, and AIM study, *Int. J. New. Chem*. **2024**, *11*, 15-33. https://doi.org/10.22034/ijnc.2023.2010699.1358.

[43] Rezaei-Sameti, M.; Kakaei, P., Evaluating the drug delivery potential of graphene, BC_3, and NC_3 nanoflakes for cyclophosphamide: A computational study analyzing static electric field and solvent effects through DFT, TD-DFT, and NLO techniques, *Comput. Theo. Chem*. **2024**, *1237*, 114659. https://doi.org/10.1016/j.comptc.2024.114659.

[44] Rezaei-Sameti, M.; Khani, H., The Effects of the Ionic Field Strength of Be^{2+}, Mg^{2+}, and Ca^{2+} and a Static Electric Field (SEF) on the Interaction Between Prothionamide and $B_{12}P_{12}$ Nanocage: A DFT and TD-DFT Study, *Phys. Chem. Res*. **2022**, *10*, 89-104. 10.22036/pcr.2021.292510.1930.

[45] Mehraein, G.; Rezaei-Sameti, M.; Asgary, E.; Aghamohammadi, M., The effects of Cu, Zn doped, and

static electrical field on the interaction of mercaptopyridine drug with B_{12} P_{12} nanocage: Insight from DFT, TD-DFT, *J. Mol. Stru*. **2022**, *1248*, 131478. https://doi.org/10.1016/j.molstruc.2021.131478.

[46] Alvand, R.; Rezaei-Sameti, M., The H^+ ions and static electric field effects on the adsorption and detection of cyanogen fluoride on the surface of boron nitride nanocage: a DFT, TD-DFT study, *Adsorption*, **2021**, *27*, 91-104. https://doi.org/10.1007/s10450-020-00278-5.

[47] Rezaei-Sameti, M.; Zanganeh, H., TD-DFT, NBO, AIM, RDG and Thermodynamic Studies of Interactions of 5-Fluorouracil Drug with Pristine and P-doped $Al_{12}N_{12}$ Nanocage, *Phys. Chem. Res.*, **2020**, *8*, 511-527. 10.22036/pcr.2020.213588.1714.

[48] Laury, M. L.; Wilson, A. K., Performance of Density Functional Theory for Second Row (4d) Transition Metal Thermochemistry, *J. Chem. Theo. Com*. **2013**, *9*, 3939-3946. https://doi.org/10.1021/ct400379z.

[49] GaussView 6.0, Gaussian, https://gaussview.software.informer.com.

[50] Chemcraft-graphical software for visualization of quantum chemistry computations. Version 1.8, build 682. https://www.chemcraftprog.com.

[51] Frisch, M. J.; *et al.* Gaussian 09, Revision D.02. Gaussian, Inc., Wallingford, CT. **2009**.

[52] Chttaraj, P. K.; Poddar, A., Molecular reactivity in the ground and excited electronic state through density-dependent local and global reactivity parameters, *J. Phys. Chem. A*. **1999**, *103*, 8691-8699. https://doi.org/10.1021/jp991214.

[53] Koopmans, T., Über die Zuordnung von Wellenfunktionen und Eigenwerten zu den einzelnen Elektronen eines Atoms, *Physica*. **1934**, *1*, 104-113. https://doi.org/10.1016/S0031-8914(34)90011-2.

[54] Bader, R. F. W.; Atoms in Molecules: A Quantum Theory, Oxford University Press, Oxford, U.K. **1990**.

[55] Johnson, E. R.; Keinan, S.; Mori Sanchez, P.; Contreras Garcia, J.; Cohen, A. J.; Yang, W., Revealing noncovalent interactions, *J. Am. Chem. Soc.* **2010**, *132*, 6498-6506. https://doi.org/10.1021/ja100936w.

[56] Savin, A., The electron localization function (ELF) and its relatives interpretations and difficulties, *J. Mol. Strut*. **2005**, *727*, 127-131. https://doi.org/10.1016/j.theochem.2005.02.034.

[57] Liu, L.; Miao, L.; Li, L.; Li, F.; Lu, Y.; Shang, Z.; Chen, J., Molecular Electrostatic Potential: A New Tool to Predict the Lithiation Process of Organic Battery Materials, *J. Phys. Chem. Lett.* **2018**, *9*, 3573-3579. https://doi.org/10.1021/acs.jpclett.8b01123.

[58] Gregory, T. C.; Reed, C. D.; David, L. K.; Mark, B. M.; Angela, M., Intrinsic fluorescence of UV-irradiated DNA. *J. Photochem. Photobiology A: Chem.* **2023**, *437*, 114484.https://doi.org/10.1016/j.jphotochem.2022.114484.

[59] Cossi, M.; Barone, V., Time-dependent density functional theory for molecules in liquid solutions, *J. Chem. Phys*. **2001**, *115*, 4708-4717. https://doi.org/10.1063/1.1394921.

[60] Pitt, I. G.; Gilbert, R. G.; Ryan, K. R., Application of Transition-State Theory to Gas-Surface Reactions: Barrierless Adsorption on Clean Surfaces, *J. Phys. Chem*. **1994**, *98*, 13001-13010. https://doi.org/10.1021/j100100a031.

[61] Tomasi, J.; Mennucci, B.; Cammi, R., Quantum Mechanical Continuum Solvation Models, *Chem. Rev.* **2005**, *105*(8), 2999-3094. https://doi.org/10.1021/cr9904009.

[62] Cossi, M.; Rega, N.; Scalmani, G.; Barone, V., Energies, structures, and electronic properties of molecules in solution with the C-PCM solvation model. *J. Comput. Chem*. **2003**, *24*(6), 669-681. https://doi.org/10.1002/jcc.10189.

[63] O'Boyle, N. M.; Tenderholt, A. L.; Langner, K. M., cclib: A library for package-independent computational chemistry algorithms, Gauss Sum, *J. Comp. Chem*., **2008**, *29*, 839-845. https://doi.org/10.1002/jcc.20823.

[64] Parr, R. G.; Pearson, R. G., Absolute hardness: companion parameter to absolute electronegativity, *J. Am. Chem. Soc.* **1983**, *105*, *7512*-7516. https://doi.org/10.1021/ja00364a005.

[65] Lu, T.; Chen, F., Multiwfn: a multifunctional wavefunction analyzer, Multiwfn: a multifunctional wavefunction analyzer. *J. Comput. Chem*. **2012**, *33*, 580-592. https://doi.org/10.1002/jcc.22885.